Synergistic modulation of the metal-free photocatalysts by composition ratio change and heteroatom doping for overall water splitting

*Jianxiong Tian†, Zhaobo Zhou†, Sheng Zhang, Zhixia Li, Li Shi *, Qiang Li *, and Jinlan Wang **

School of Physics, Southeast University, Nanjing 211189, China

* E-mail: jlwang@seu.edu.cn.

1. Calculation methods of OER activity and adsorption energy of *O and *OH

(1) Calculation method of OER activity

The OER activity is assessed by calculating the reaction free energy of each step based on some thermal corrections:

In our work, the computational hydrogen electrode (CHE) model is applied.[1] At U=0 V, $\Delta G = \Delta E + \Delta E_{ZPE} - T\Delta S + \int C_P dT + \Delta G_{pH}$, where ΔE is the reaction energy difference between the product and reactant of the OER occurring on catalysts, which can be directly obtained from DFT computations; ΔE_{ZPE}, $T\Delta S$ and $\int C_P dT$ are zero-point energy correction, entropy correction and enthalpic temperature correction at T=298.15 K respectively, which can be calculated from the vibrational frequencies. ΔG_{pH} is the free energy of correction of pH, which can be calculated by $\Delta G_{pH} = K_B T \times pH \times \ln 10$, and the pH value is set to be zero for strong acidic medium

in this work. The ΔE_{ZPE}, $T\Delta S$ and $\int C_P dT$ for each reaction intermediates can be calculated by the following equations, respectively:

$$E_{ZPE} = \frac{1}{2}\sum_i h\nu_i \quad (S1)$$

$$-TS = K_B T \sum_i \ln\left(1 - e^{-\frac{h\nu_i}{K_B T}}\right) - \sum_i h\nu_i \left(\frac{1}{e^{\frac{h\nu_i}{K_B T}} - 1}\right) \quad (S2)$$

$$\int C_P dT = \sum_i h\nu_i \left(\frac{1}{e^{\frac{h\nu_i}{K_B T}} - 1}\right) \quad (S3)$$

In the equations above, h, ν and K_B are Planck constant, vibrational frequencies and Boltzmann constant, respectively. Only vibration modes of the adsorbates were taken into account for thermodynamic corrections, assuming that changes in the vibrations of the catalyst surface caused by the presence of the carbon nitrides were minimal.[2, 3] Therefore, the free energy for each step of OER can be calculated by:

(i) $H_2O(l) + * \rightleftharpoons *OH + H^+ + e^-$ $(S4)$

$$\Delta G_1 = G_{*OH} + G_{H^+} + G_{e^-} - G_* - G_{H_2O} = G_{*OH} + \frac{1}{2}G_{H_2} + G_* - G_{H_2O} \quad (S5)$$

(ii) $*OH \rightleftharpoons *O + H^+ + e^-$ $(S6)$

$$\Delta G_2 = G_O + G_{H^+} + G_{e^-} - G_{*OH} = G_O + \frac{1}{2}G_{H_2} - G_{*OH} \quad (S7)$$

(iii) $*O + H_2O(l) \rightleftharpoons *OOH + H^+ + e^-$ $(S8)$

$$\Delta G_3 = G_{*OOH} + G_{H^+} + G_{e^-} - G_{*O} - G_{H_2O} = G_{*OOH} + \frac{1}{2}G_{H_2} - G_{*O} - G_{H_2O} \quad (S9)$$

(iv)

$*OOH \rightleftharpoons * + O_2(g) + H^+ + e^-$ $(S10)$

$$\Delta G_4 = 4.92 - \Delta G_1 - \Delta G_2 - \Delta G_3 \quad (S11)$$

The overpotential, which is determined by the rate determining step, is calculated by the formula:

$$\eta = max[\Delta G_1, \Delta G_2, \Delta G_3, \Delta G_4] / e - 1.23 \quad (S12)$$

(2) Calculation method of adsorption energy of *O and *OH

The adsorption energies of *O and *OH are obtained as follows:

$$\Delta E_{OH} = E_{*OH} - E_* - (E_{H_2O} - \frac{1}{2}E_{H_2}) \quad (S13)$$

$$\Delta E_O = E_{*O} - E_* - (E_{H_2O} - E_{H_2}) \quad (S14)$$

In $(S13)$ and $(S14)$, ΔE_{OH} and ΔE_O are the adsorption energy of OH and O and E_{*OH}, E_* and E_* are the energies of a clean catalyst and the catalyst adsorbed with OH, O and OOH, respectively. E_{H_2O} and E_{H_2} is the energy calculated via DFT.

2. Figures

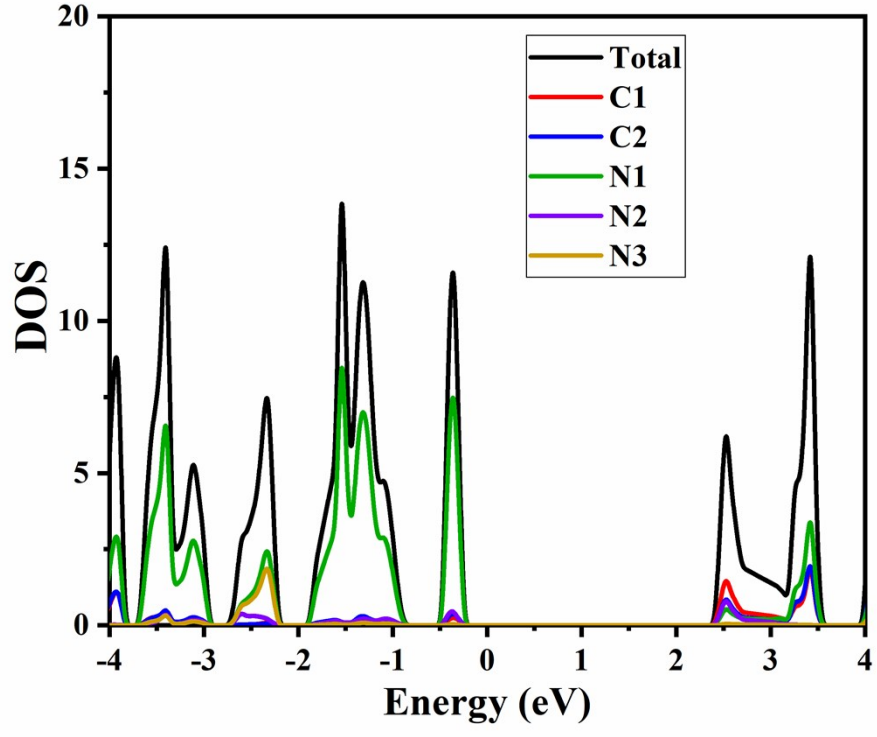

Fig. S1. The projected density of states of g-C_3N_4 relative to Fermi level by HSE06.

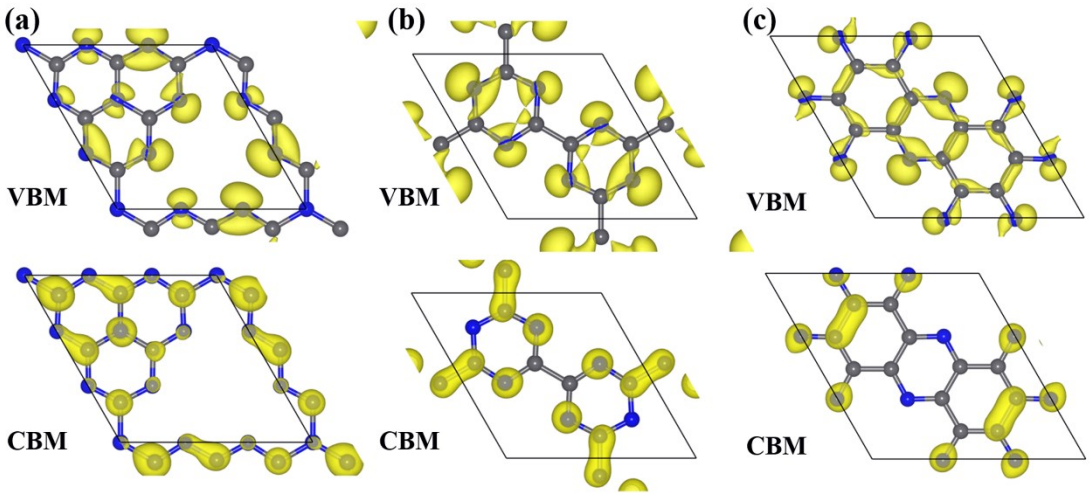

Fig. S2. Charge density distributions of valence band maximum (VBM) and conduction band minimum (CBM) for (a) g-C_3N_4, (b) g-C_3N_3 and (c) g-C_2N, respectively. The isosurface value is 0.007 e/Bohr^3.

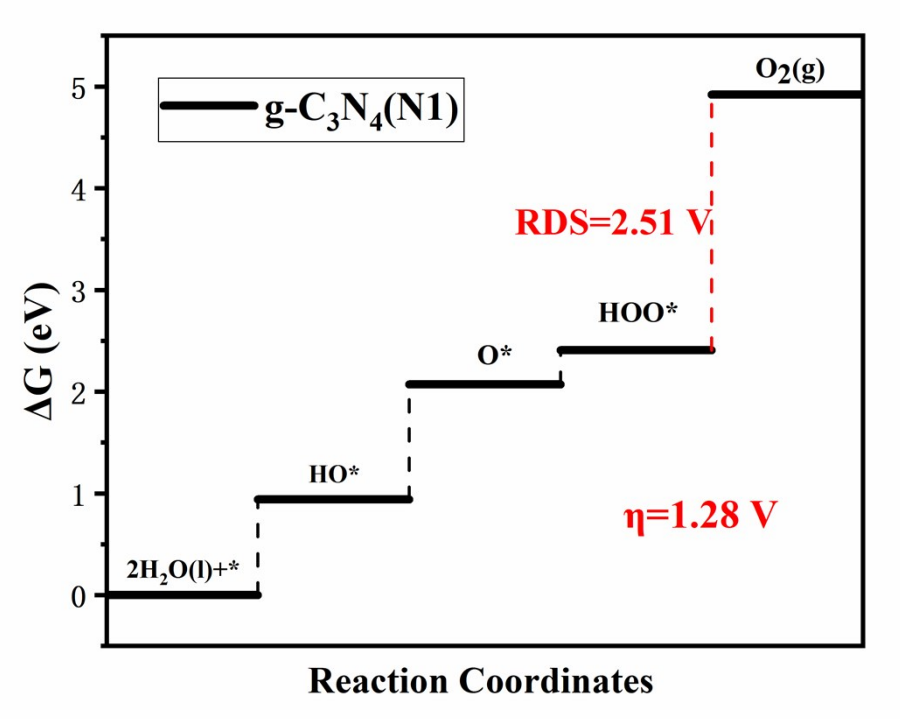

Fig. S3. Free energy diagram of pristine g-C_3N_4 on N1 site at zero potential (U=0), where the rate determining step is marked by dashed line in red.

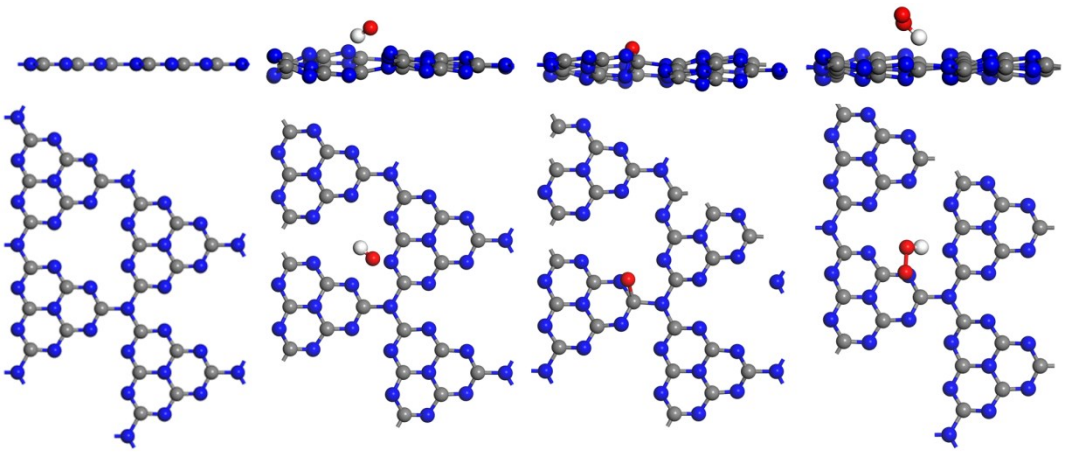

Fig. S4. Optimized structures of reaction intermediates of pristine g-C_3N_4 on N1 site during OER, where gray, blue, red, yellow balls represent C, N, O and S atoms, respectively.

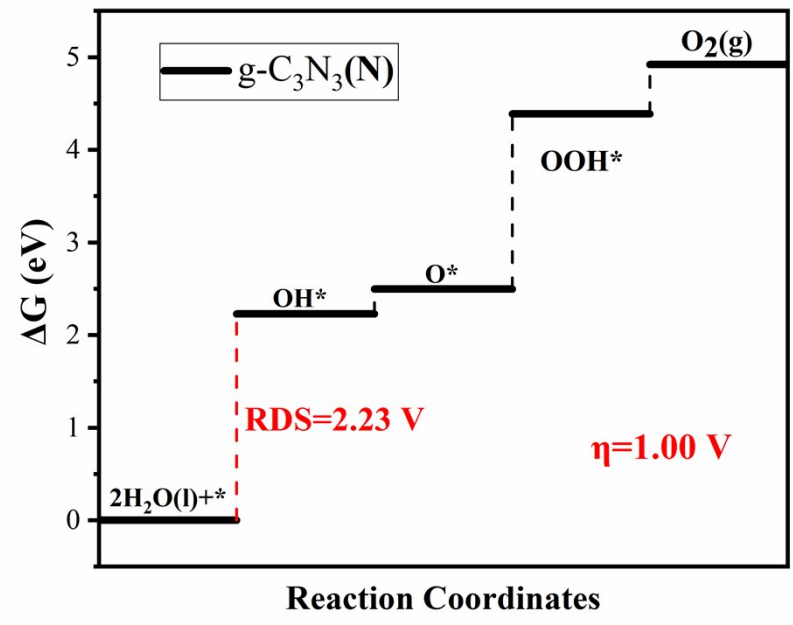

Fig. S5. Free energy diagram of pristine g-C_3N_3 on N site at zero potential (U=0), where the rate determining step is marked by dashed line in red.

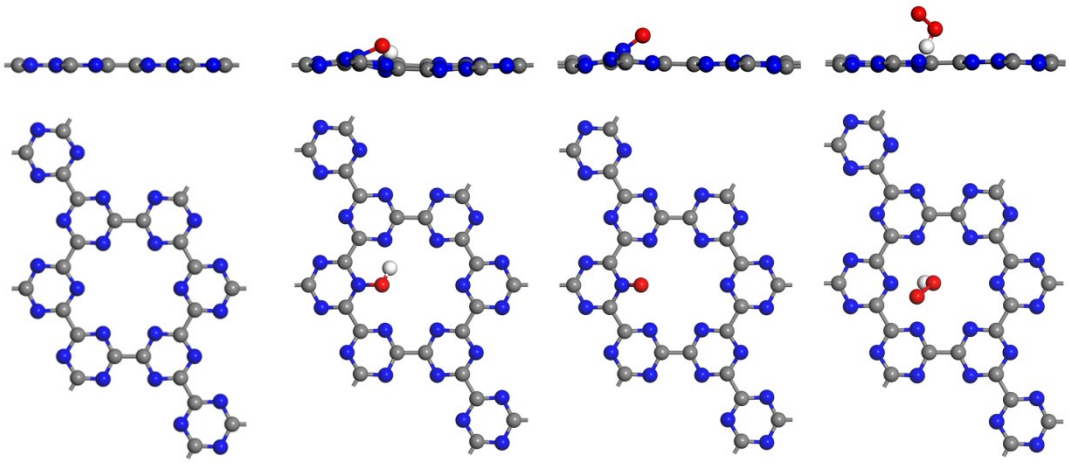

Fig. S6. Optimized structures of reaction intermediates of pristine g-C_3N_3 on N site during OER.

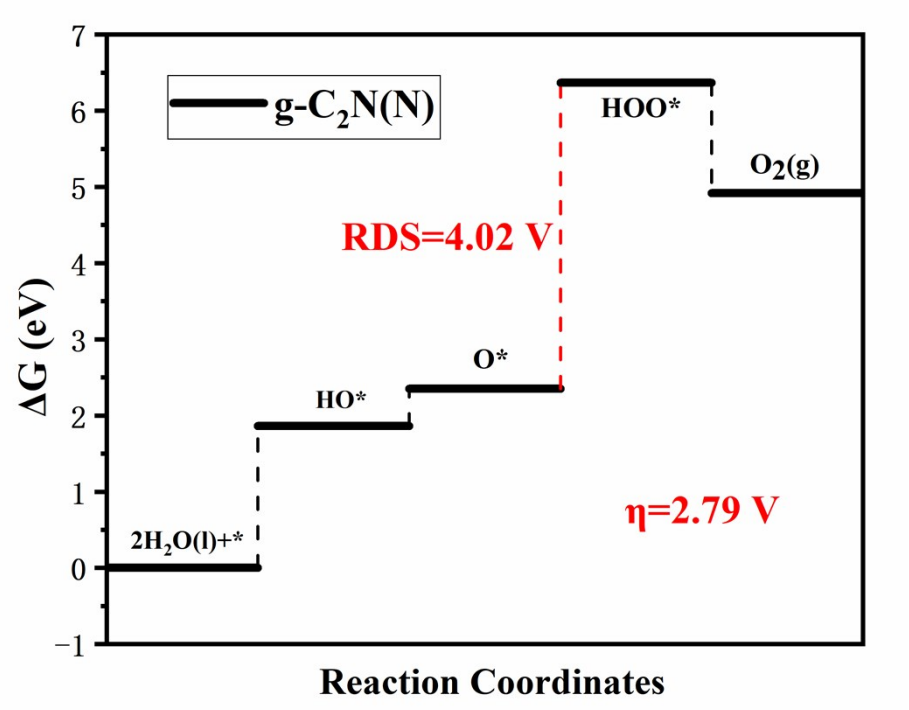

Fig. S7. Free energy diagram of pristine g-C_2N on N site at zero potential (U=0), where the rate determining step is marked by dashed line in red.

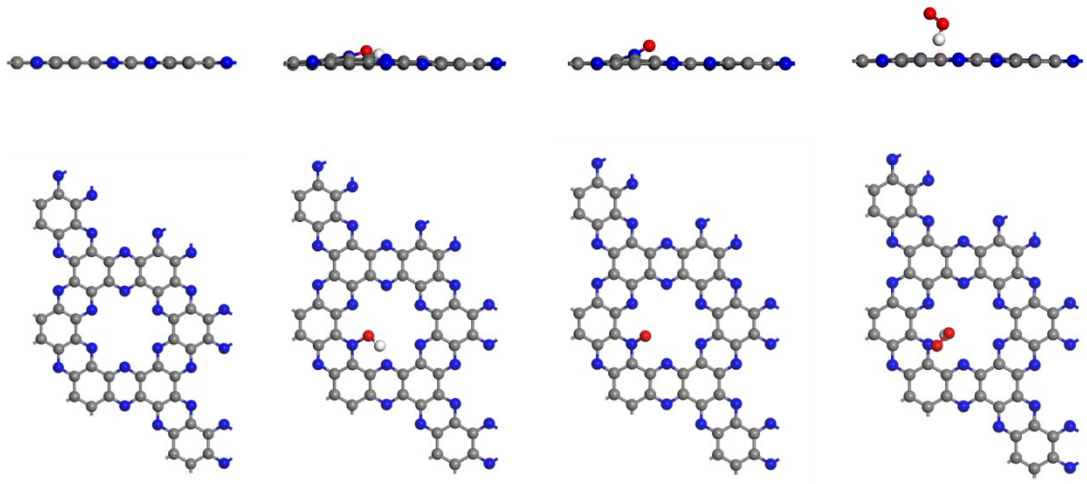

Fig. S8. Optimized structures of reaction intermediates of pristine g-C_2N on N site during OER.

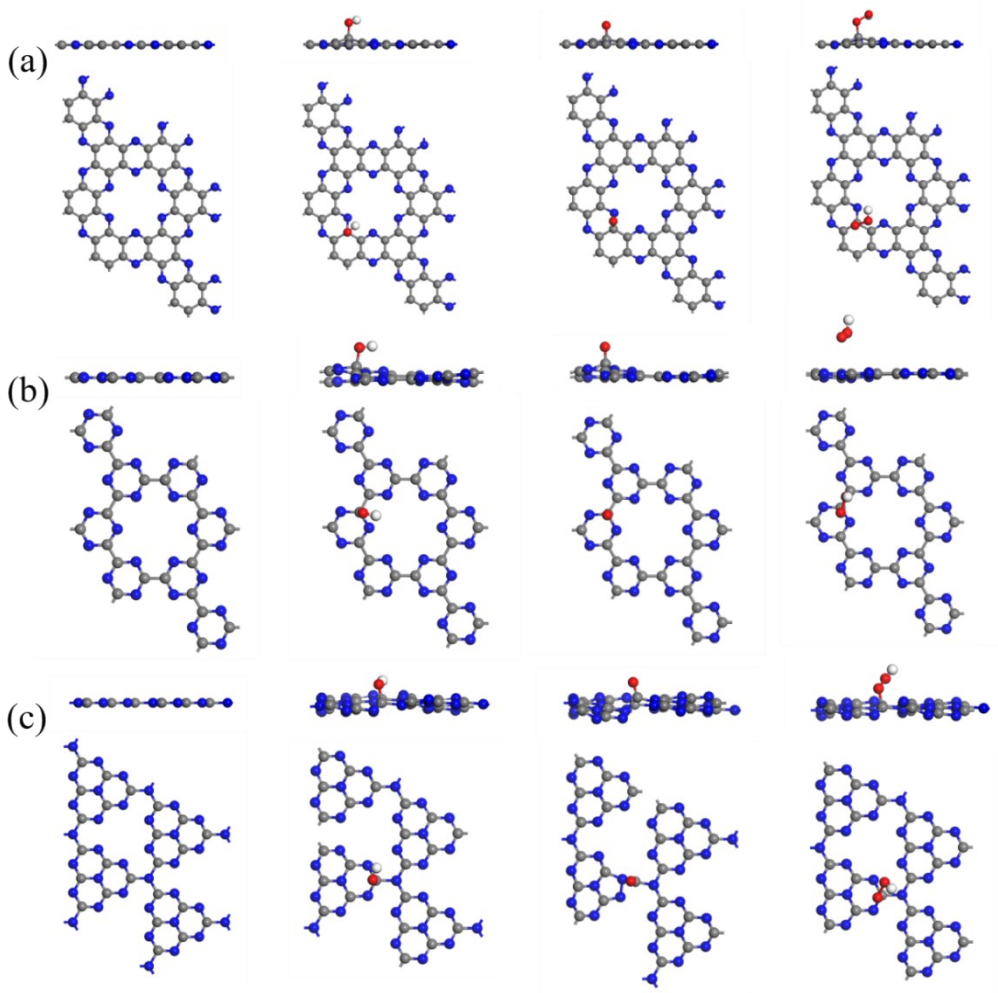

Fig. S9. Optimized structures of reaction intermediates of pristine (a) g-C_2N, (b) g-C_3N_3 and (c) g-C_3N_4 during OER.

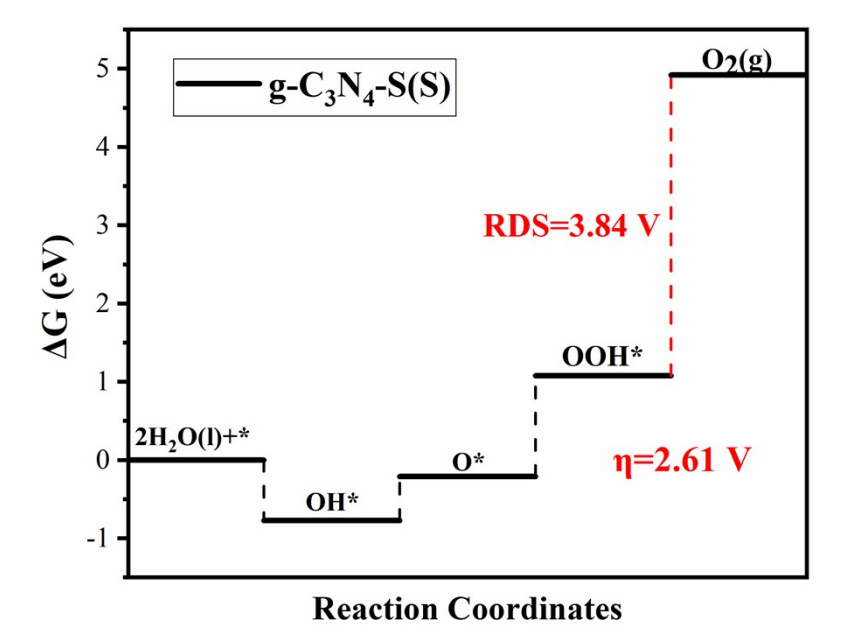

Fig. S10. Free energy diagram of S-doped g-C_3N_4 on S site at zero potential (U=0), where the rate determining step is marked by dashed line in red.

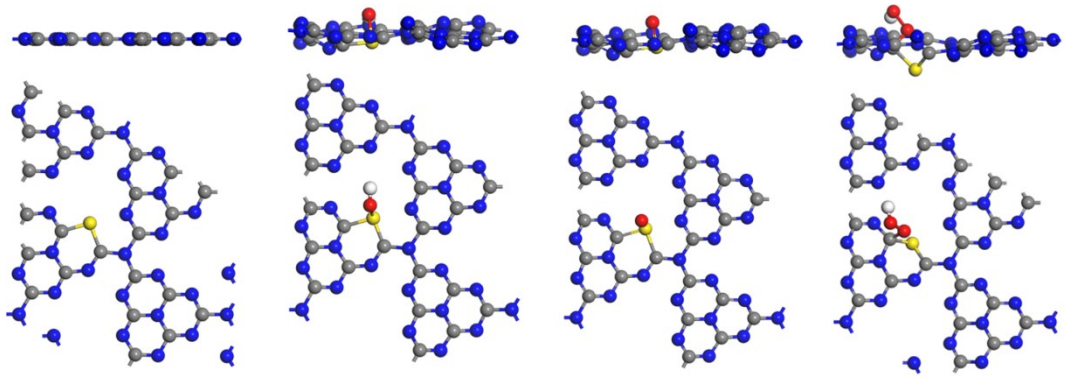

Fig. S11. Optimized structures of reaction intermediates of S-doped g-C_3N_4 on S site during OER.

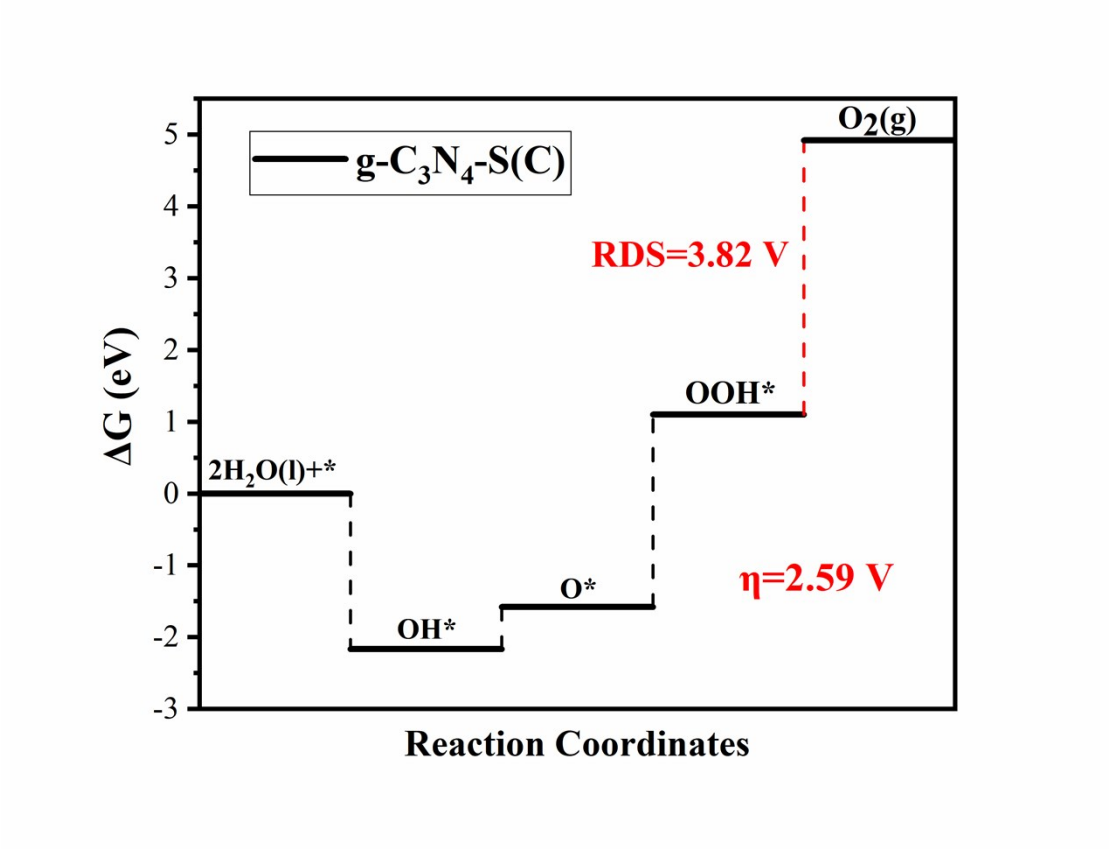

Fig. S12. Free energy diagram of S-doped g-C_3N_4 on C site at zero potential (U=0), where the rate determining step is marked by dashed line in red.

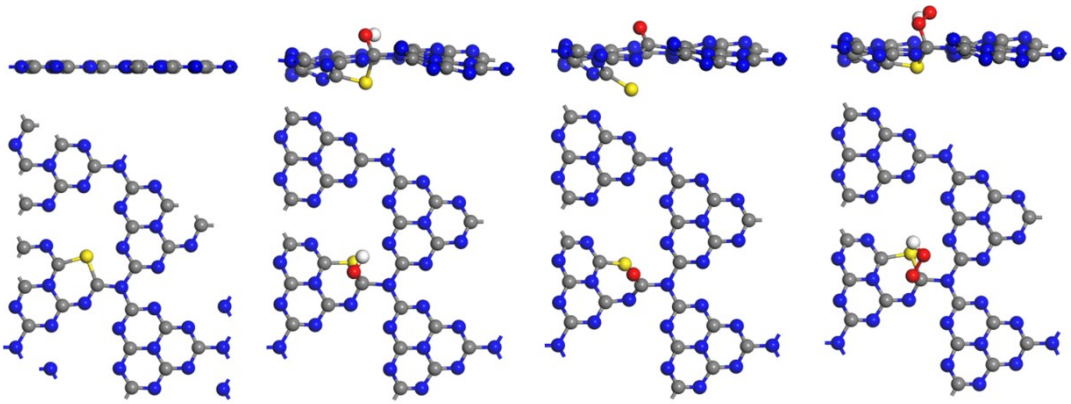

Fig. S13. Optimized structures of reaction intermediates of S-doped g-C_3N_4 on C site during OER.

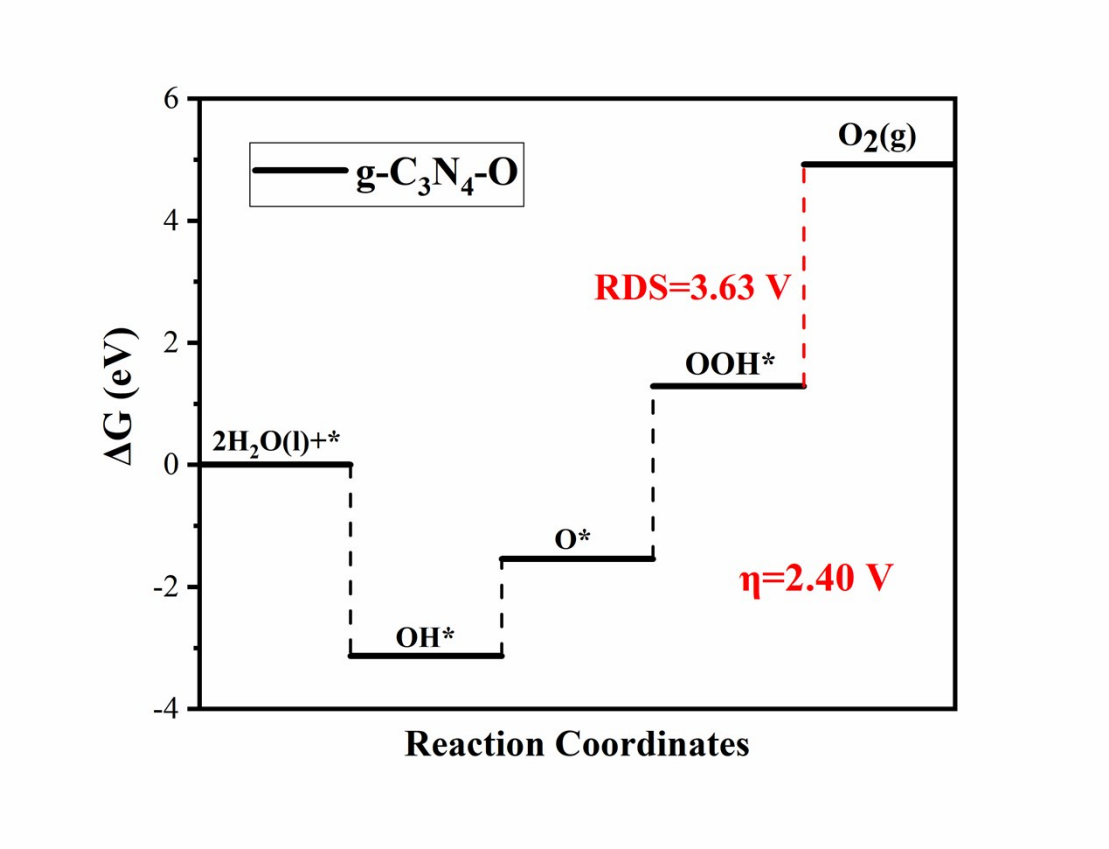

Fig. S14. Free energy diagram of O-doped g-C_3N_4 on C site at zero potential (U=0), where the rate determining step is marked by dashed line in red.

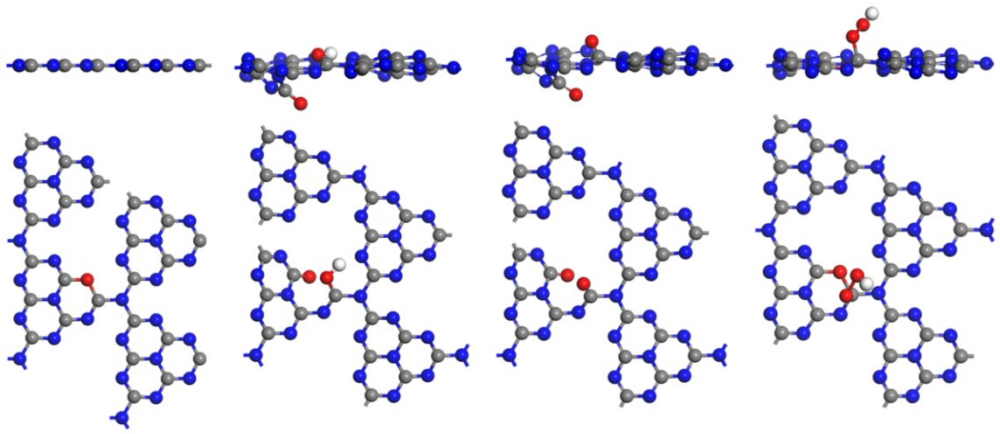

Fig. S15. Optimized structures of reaction intermediates of O-doped g-C_3N_4 on C site during OER.

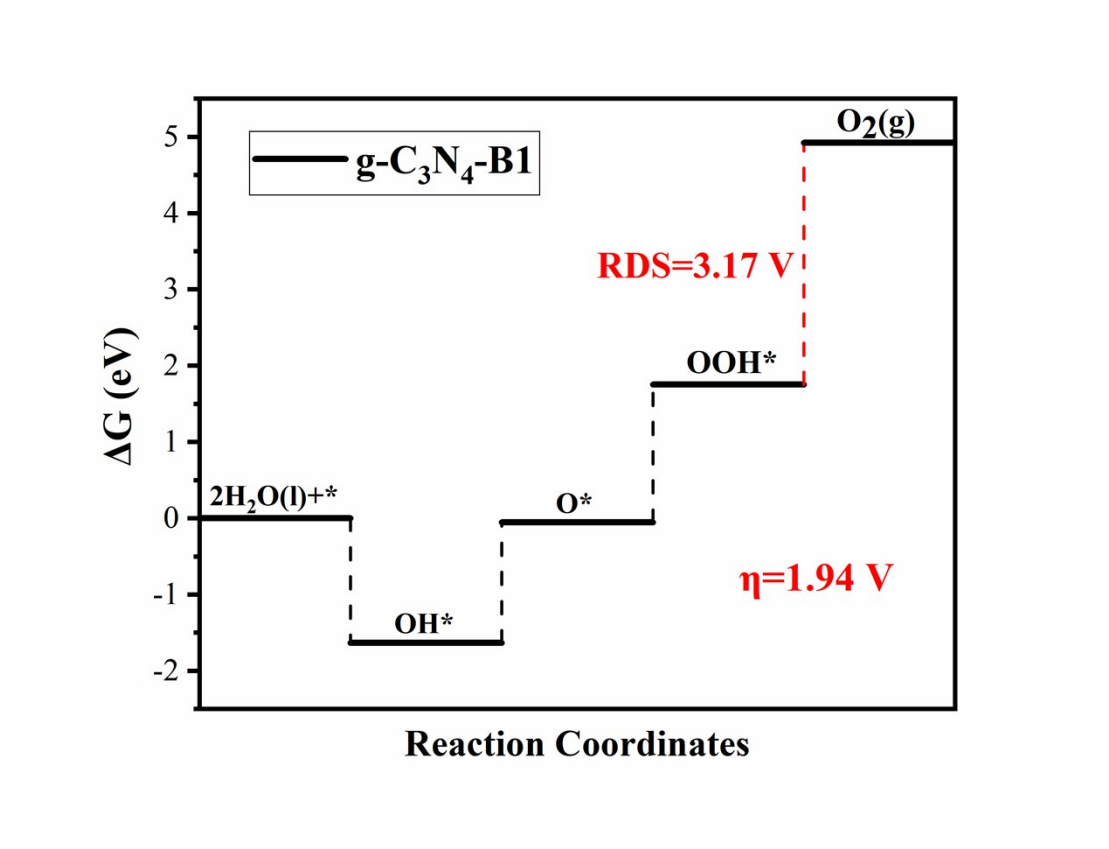

Fig. S16. Free energy diagram of B1-doped g-C_3N_4 on B1 site at zero potential (U=0), where the rate determining step is marked by dashed line in red.

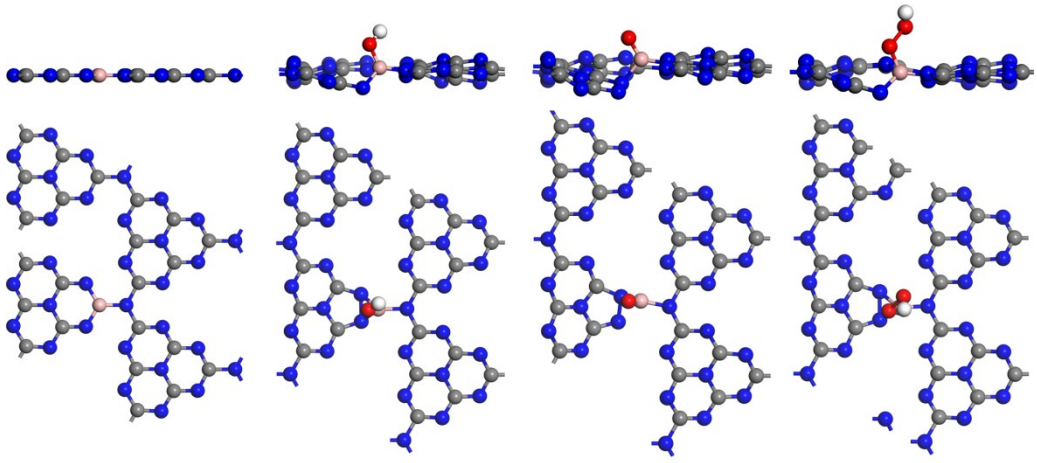

Fig. S17. Optimized structures of reaction intermediates of B1-doped g-C_3N_4 on B1 site during OER.

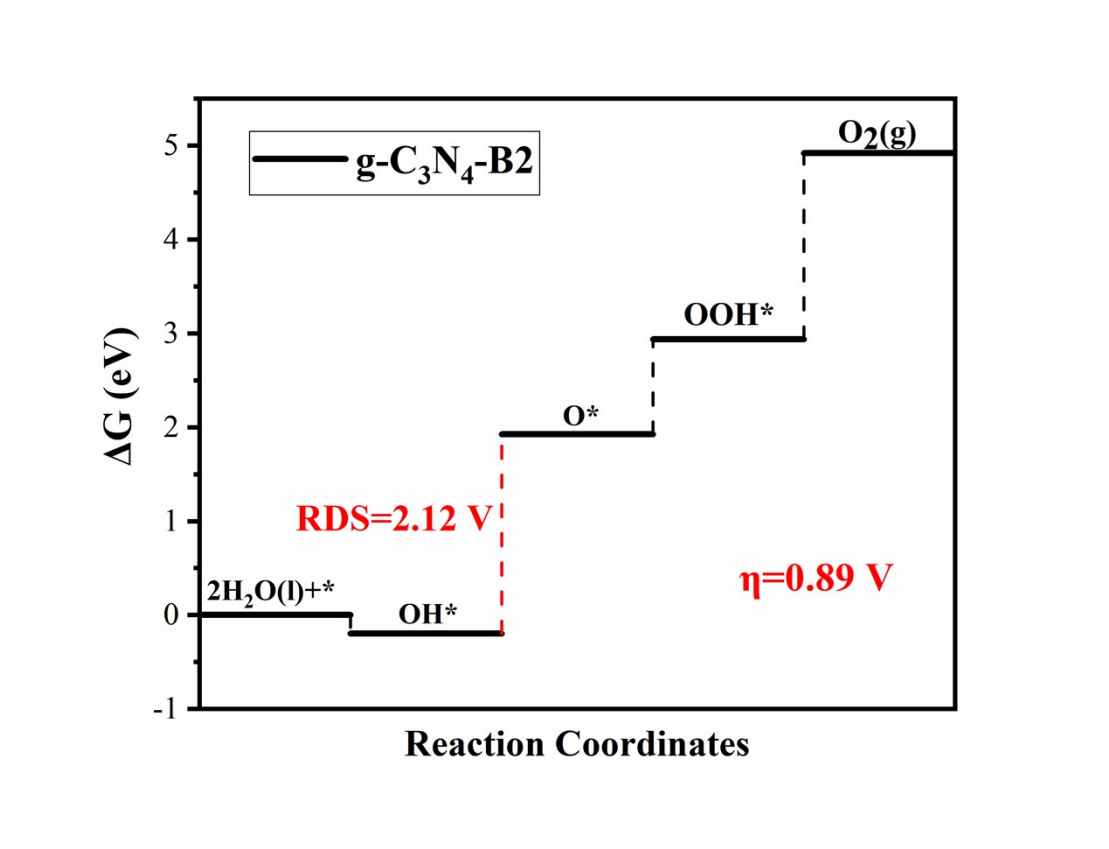

Fig. S18. Free energy diagram of B2-doped g-C_3N_4 on B2 site at zero potential (U=0), where the rate determining step is marked by dashed line in red.

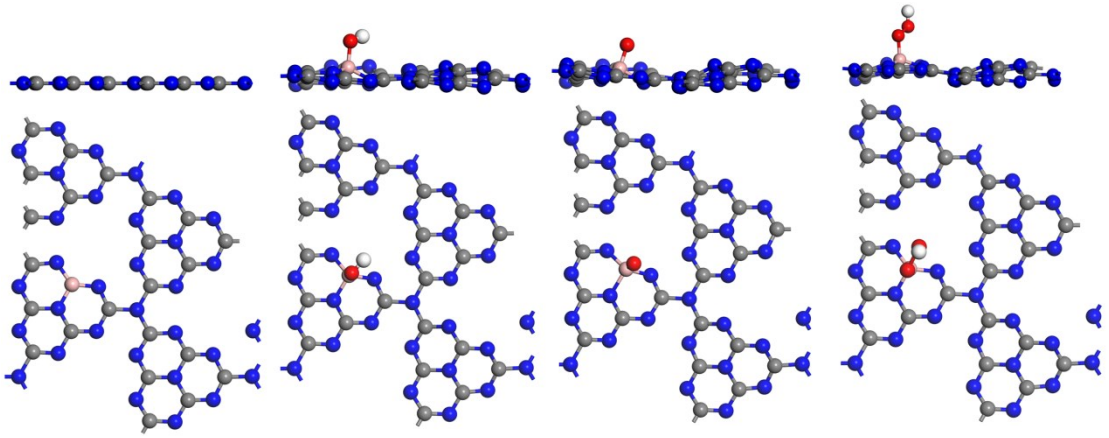

Fig. S19. Optimized structures of reaction intermediates of B2-doped g-C_3N_4 on B2 site during OER.

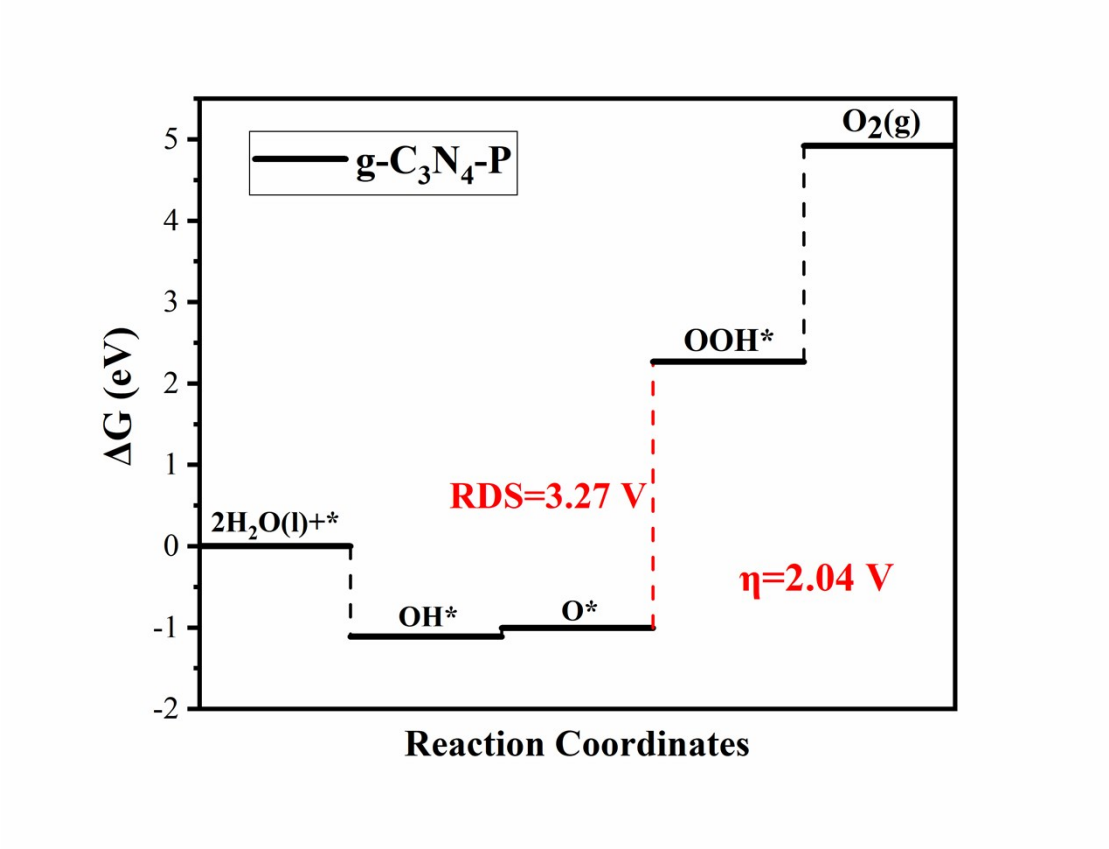

Fig. S20. Free energy diagram of P-doped g-C_3N_4 on P site at zero potential (U=0), where the rate determining step is marked by dashed line in red.

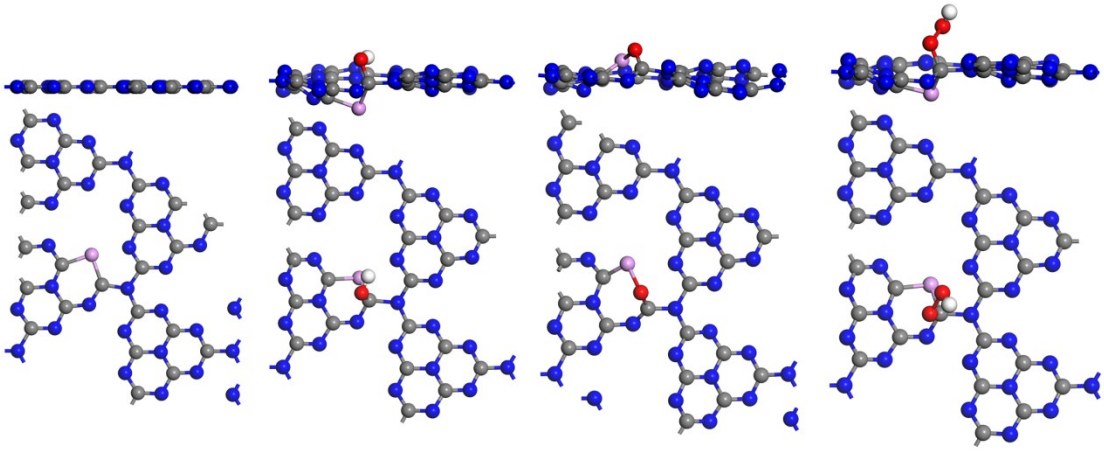

Fig. S21. Optimized structures of reaction intermediates of P-doped g-C_3N_4 on P site during OER.

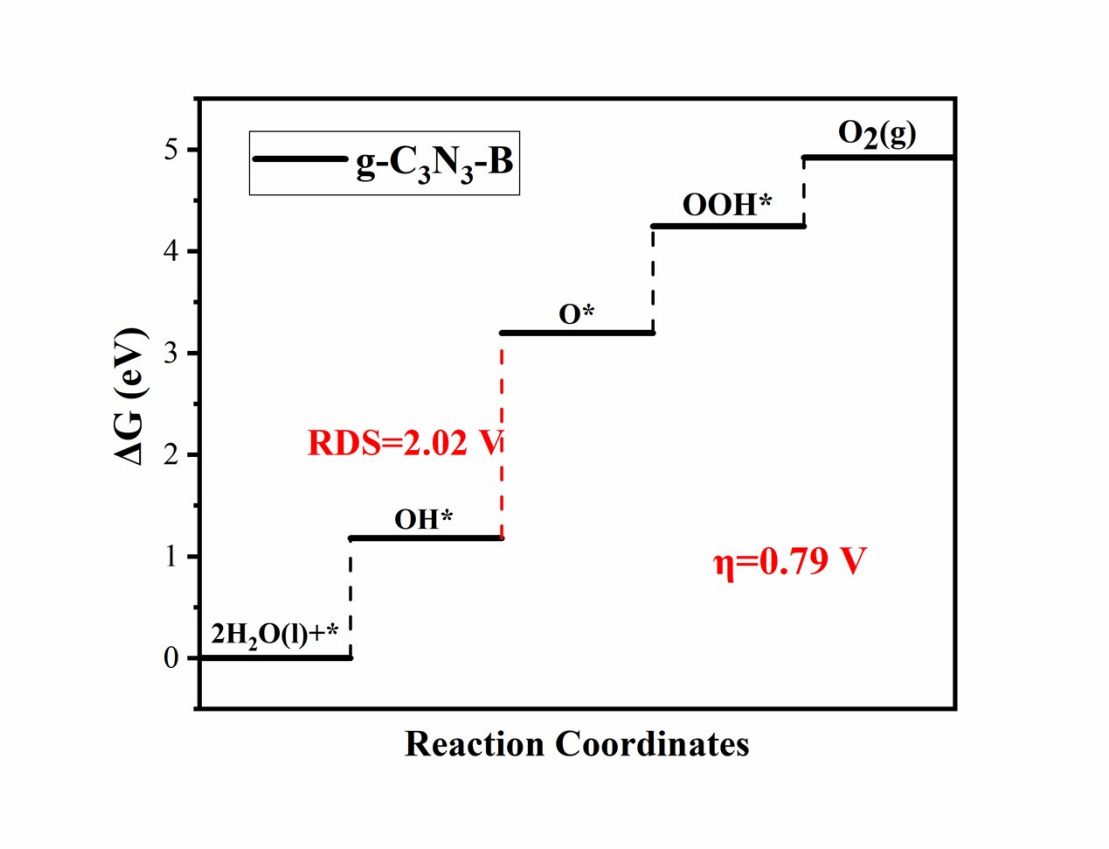

Fig. S22. Free energy diagram of B-doped g-C_3N_3 on B site. at zero potential (U=0), where the rate determining step is marked by dashed line in red.

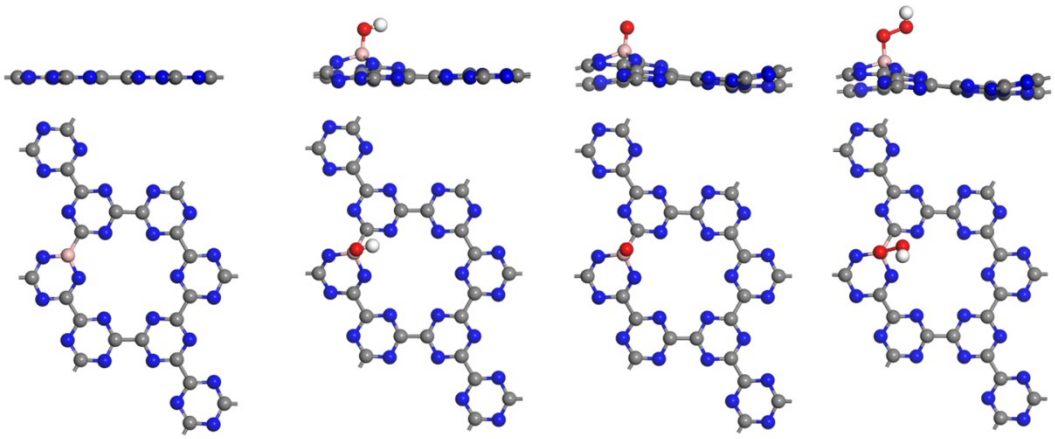

Fig. S23. Optimized structures of reaction intermediates of B-doped g-C_3N_3 on B site during OER.

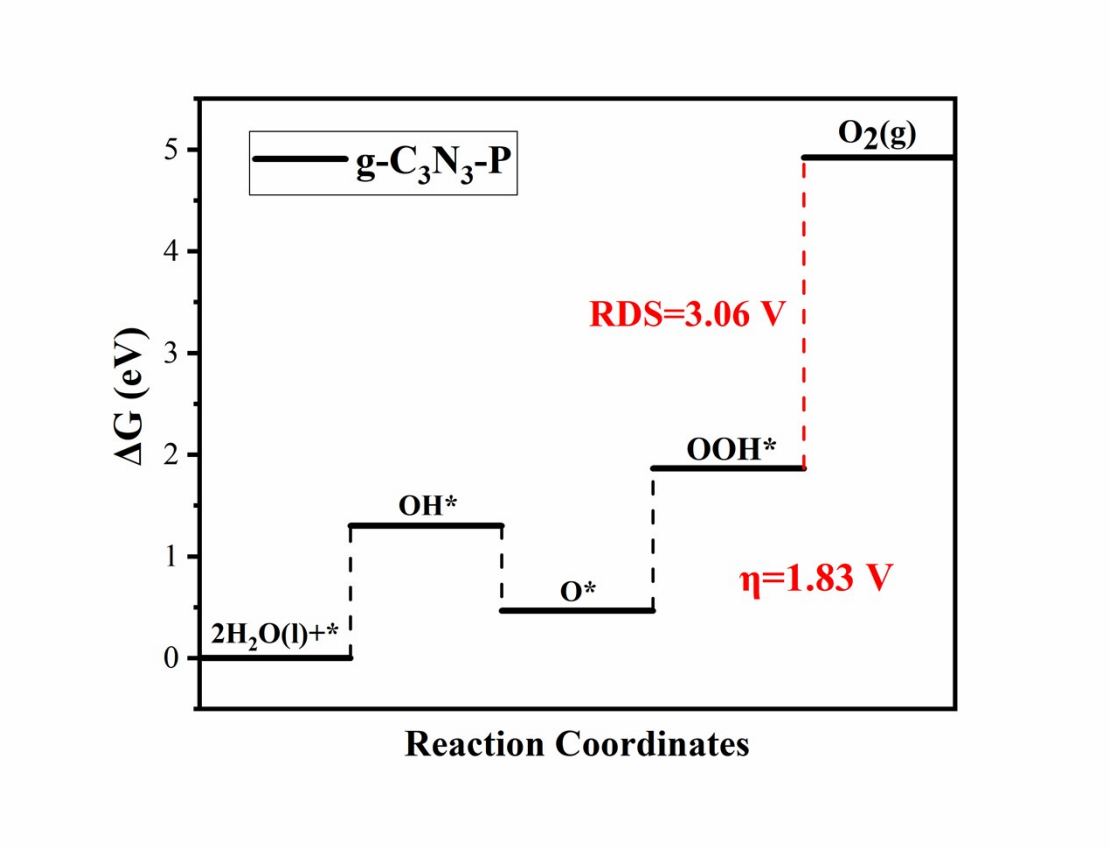

Fig. S24. Free energy diagram of P-doped g-C_3N_3 on C site. at zero potential (U=0), where the rate determining step is marked by dashed line in red.

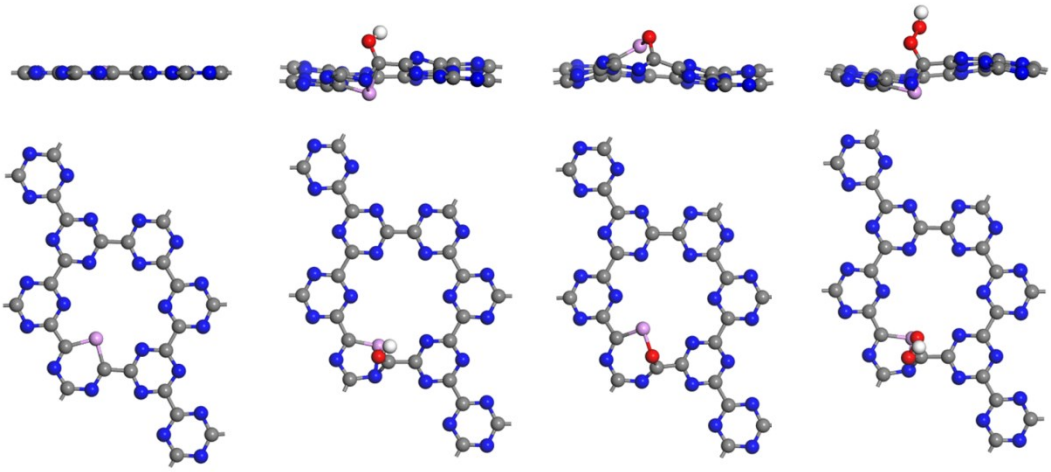

Fig. S25. Optimized structures of reaction intermediates of P-doped g-C_3N_4 on C site during OER.

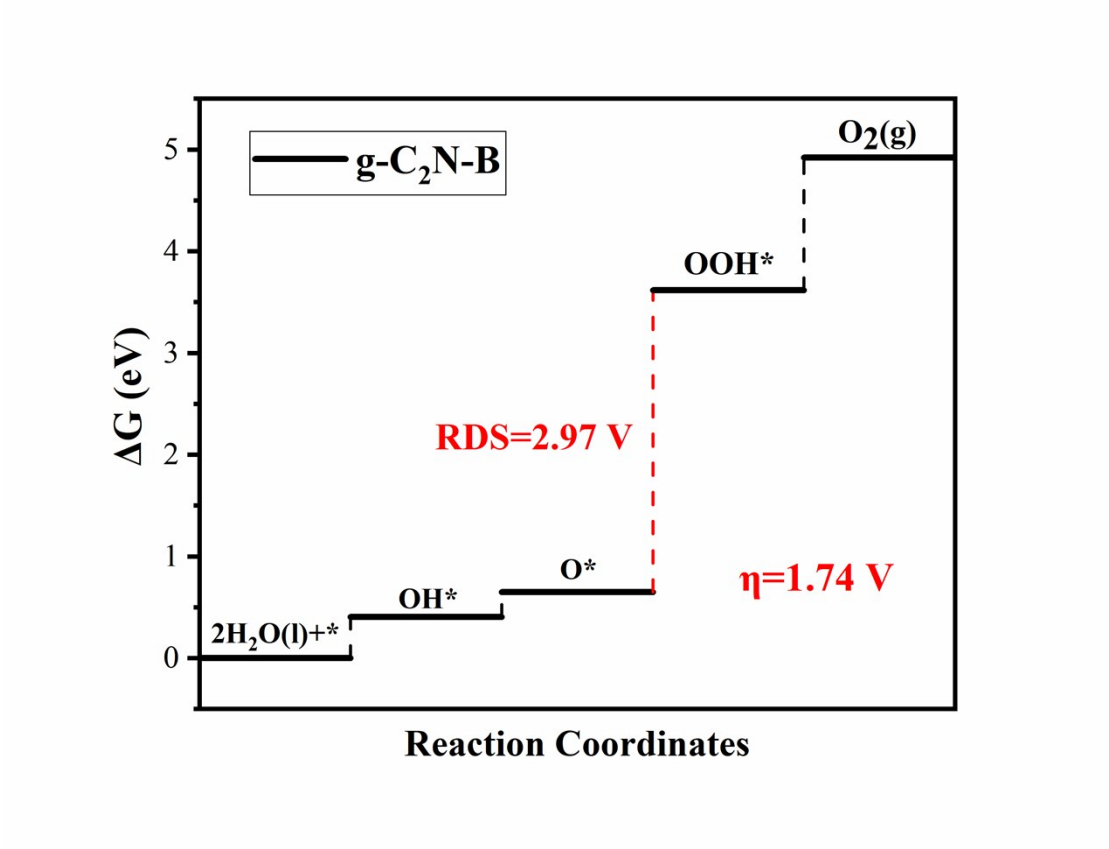

Fig. S26. Free energy diagram of B-doped g-C_2N on B site. at zero potential (U=0), where the rate determining step is marked by dashed line in red.

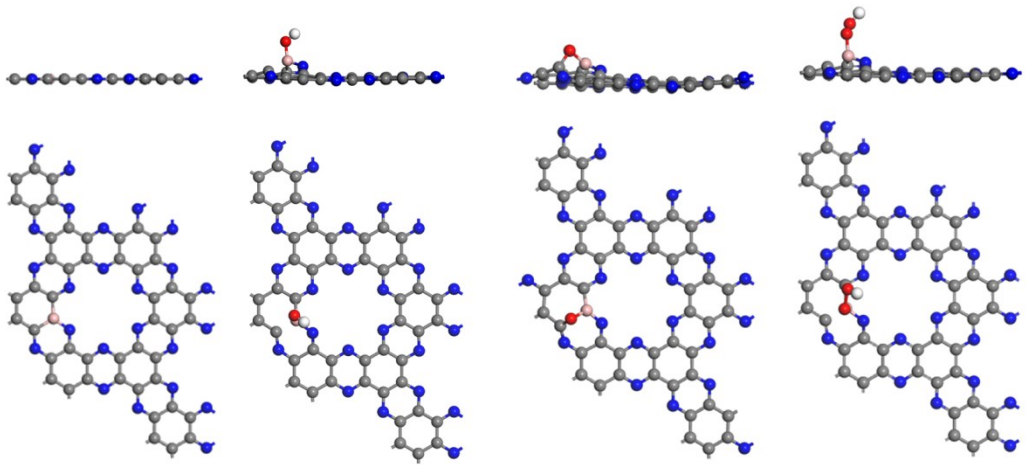

Fig. S27. Optimized structures of reaction intermediates of B-doped g-C_2N on B site during OER.

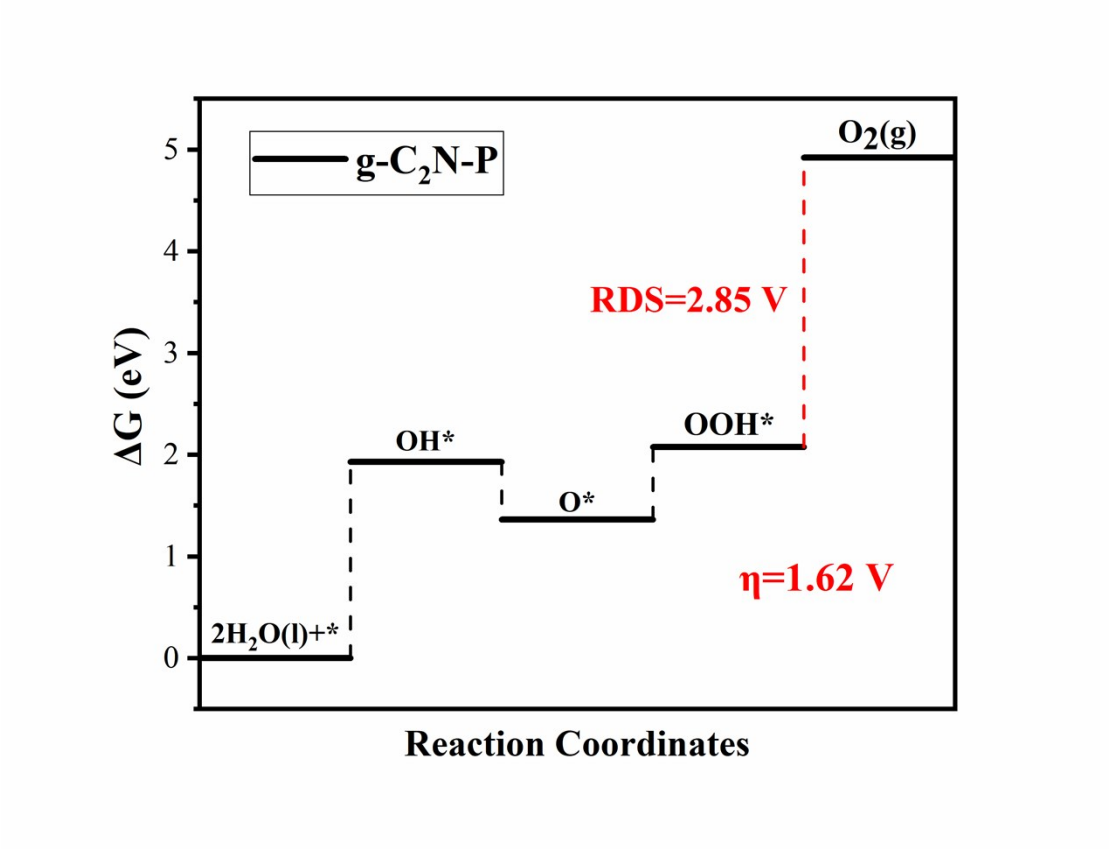

Fig. S28. Free energy diagram of P-doped g-C_2N on C site at zero potential (U=0), where the rate determining step is marked by dashed line in red.

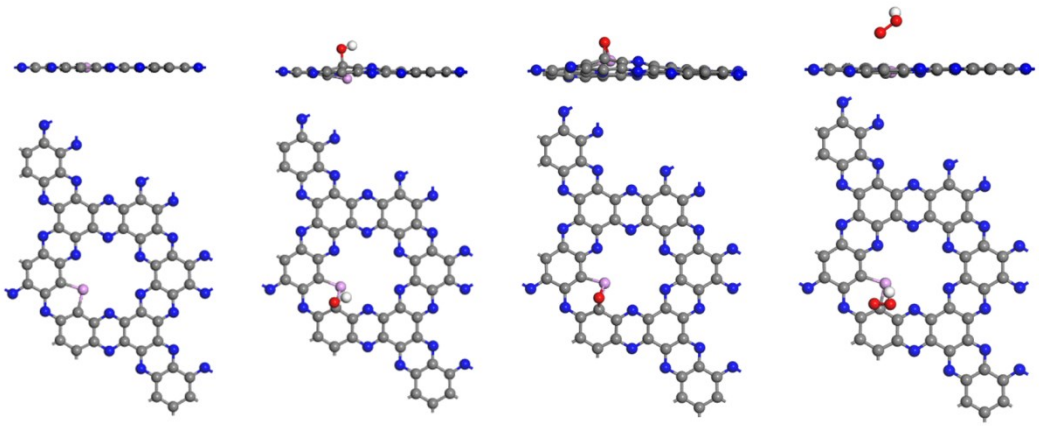

Fig. S29. Optimized structures of reaction intermediates of P-doped g-C_2N on C site during OER.

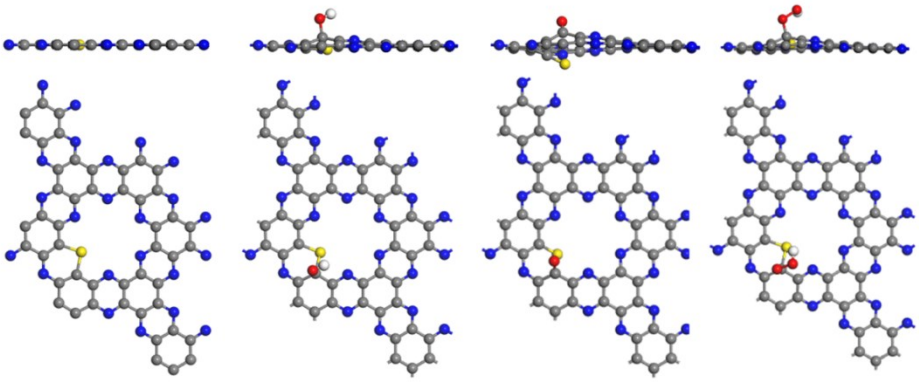

Fig. S30. Optimized structures of reaction intermediates of S-doped g-C_2N on C site during OER.

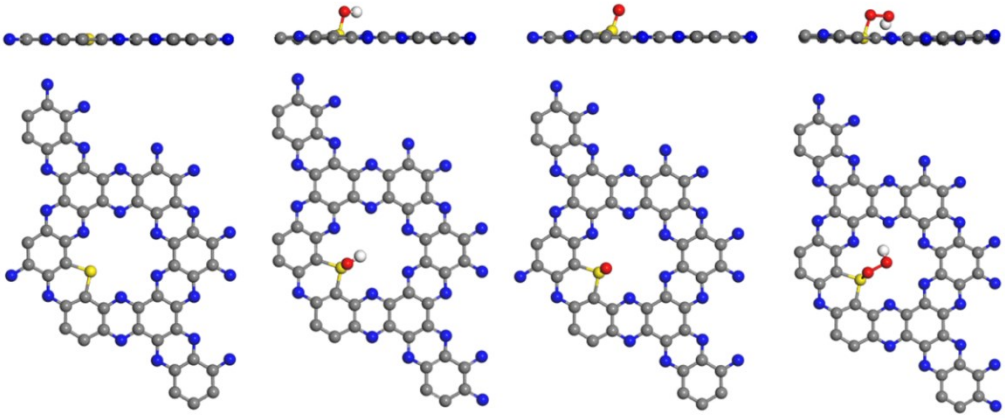

Fig. S31. Optimized structures of reaction intermediates of S-doped g-C_2N on S site during OER.

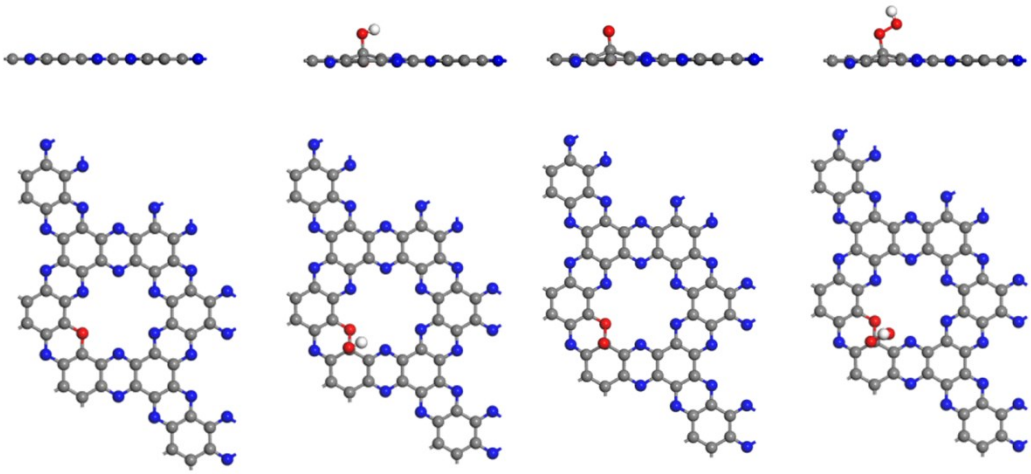

Fig. S32. Optimized structures of reaction intermediates of O-doped g-C_2N on C site during OER.

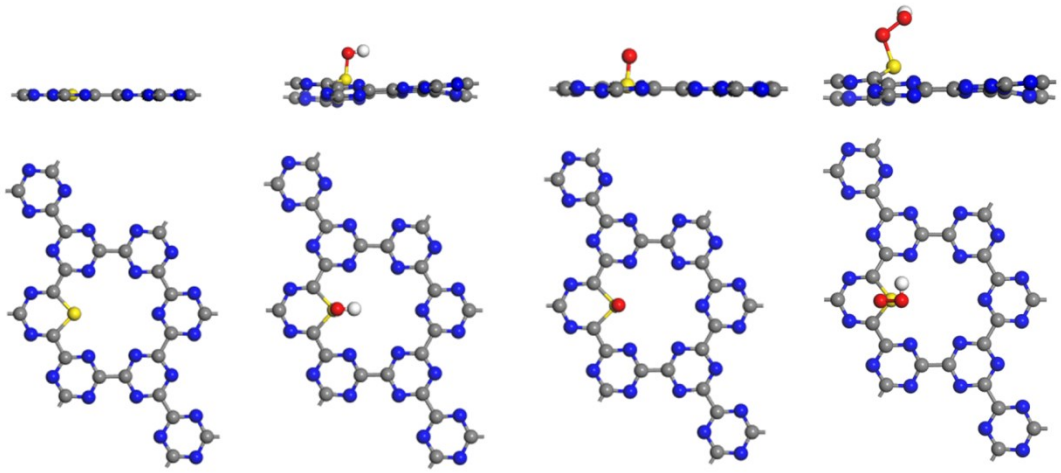

Fig. S33. Optimized structures of reaction intermediates of S-doped g-C_3N_3 on S site during OER.

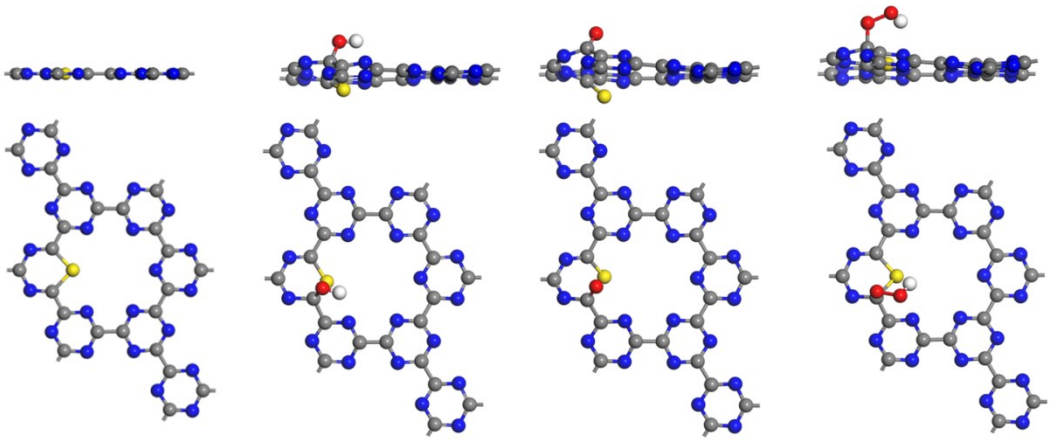

Fig. S34. Optimized structures of reaction intermediates of S-doped g-C_3N_3 on C site during OER.

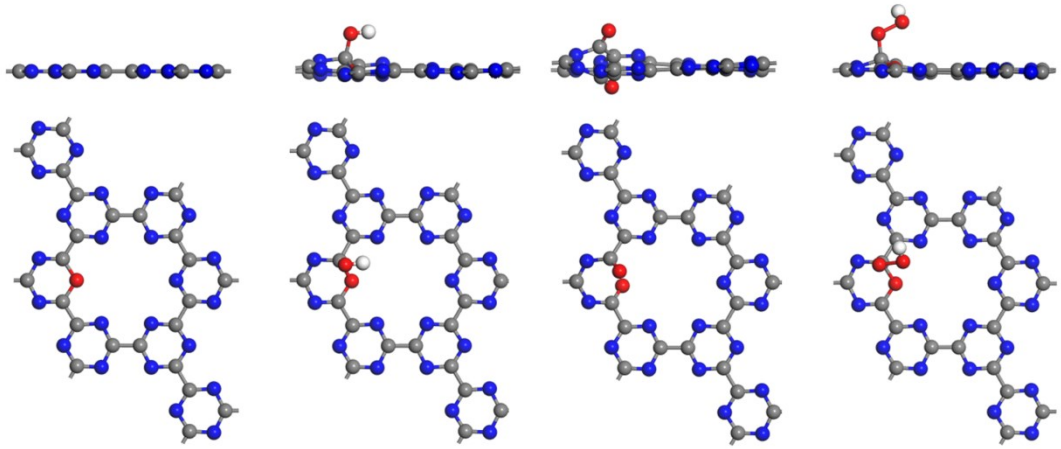

Fig. S35. Optimized structures of reaction intermediates of O-doped g-C_3N_3 on C site during OER.

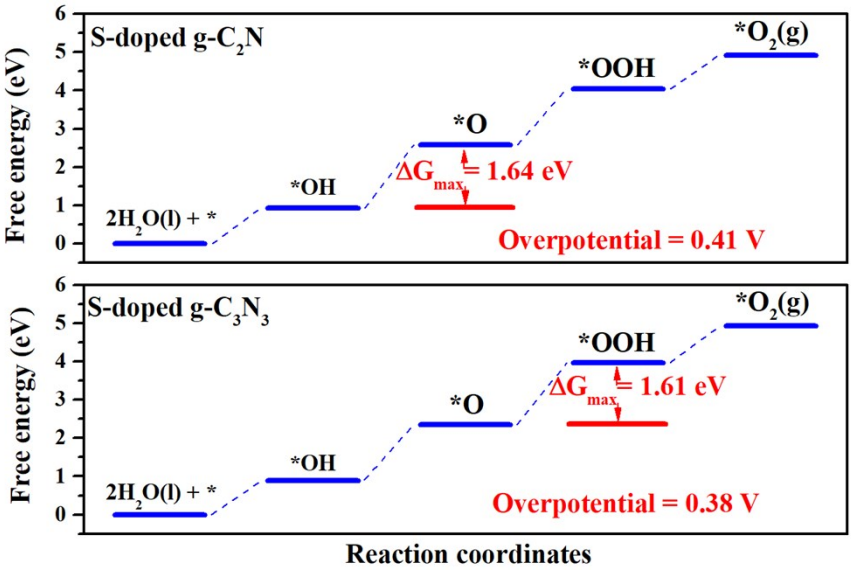

Fig. S36. Free energy diagrams of OER on S-doped g-C_2N and g-C_3N_3 with lower doping concentration.

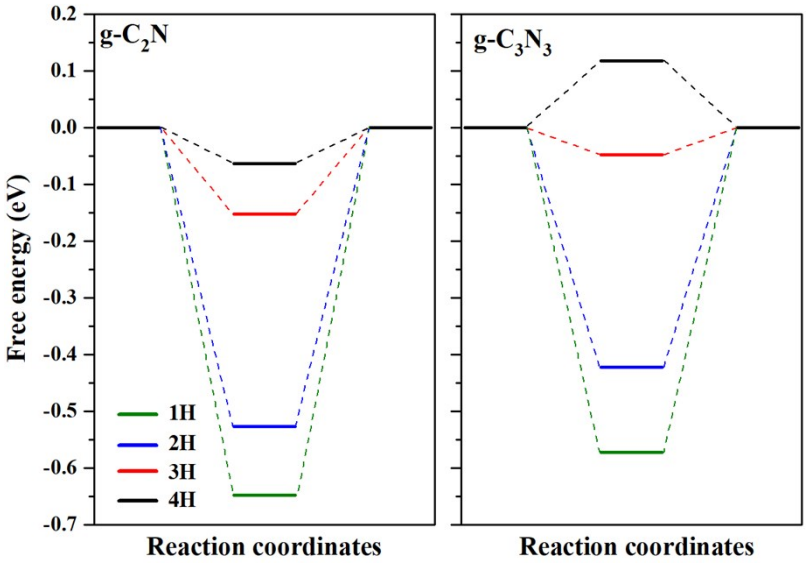

Fig. S37. Free energy difference with different hydrogen coverages on the N sites of g-C_2N and g-C_3N_3.

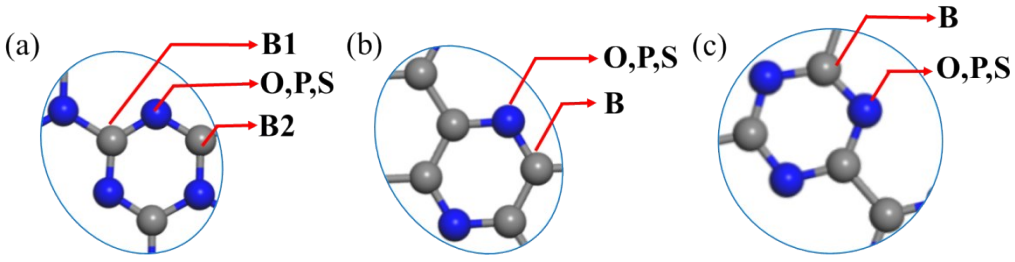

Fig. S38. Doping sites of (a) g-C_3N_4, (b) g-C_3N_3 and (c) g-C_2N. For g-C_3N_4, the doping site of O, P and S atom is on N1 atom, and the doping site of B is on C1 or C2; For g-C_3N_3 and g-C_2N, the doping site of O, P and S is on N and the doping site of B is on C.

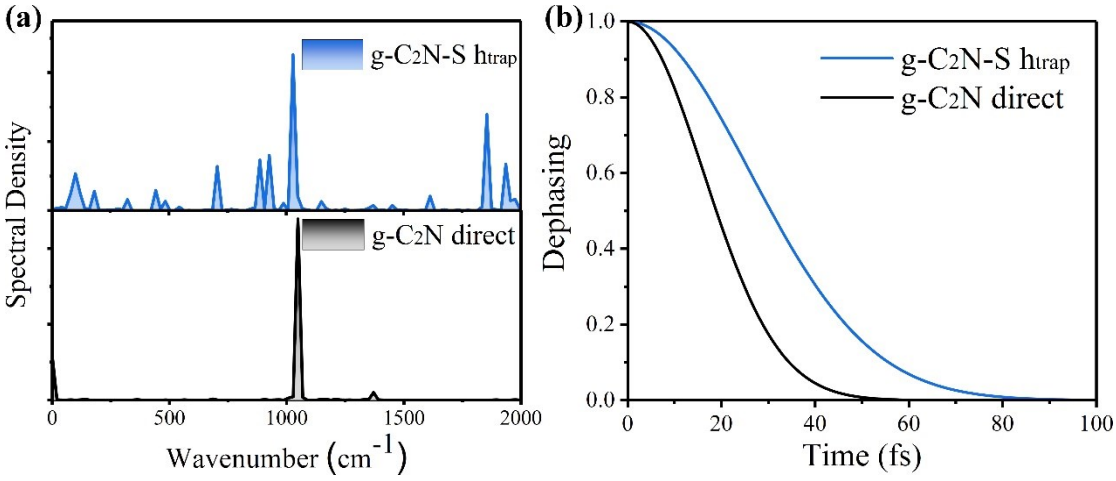

Fig. S39. (a) Fourier transforms of the energy gaps between donor and acceptor states of hole trap and direct e-h recombination dynamics for S-doped g-C_2N. (b) Pure-dephasing functions of hole trap and direct e-h recombination for S-doped g-C_2N.

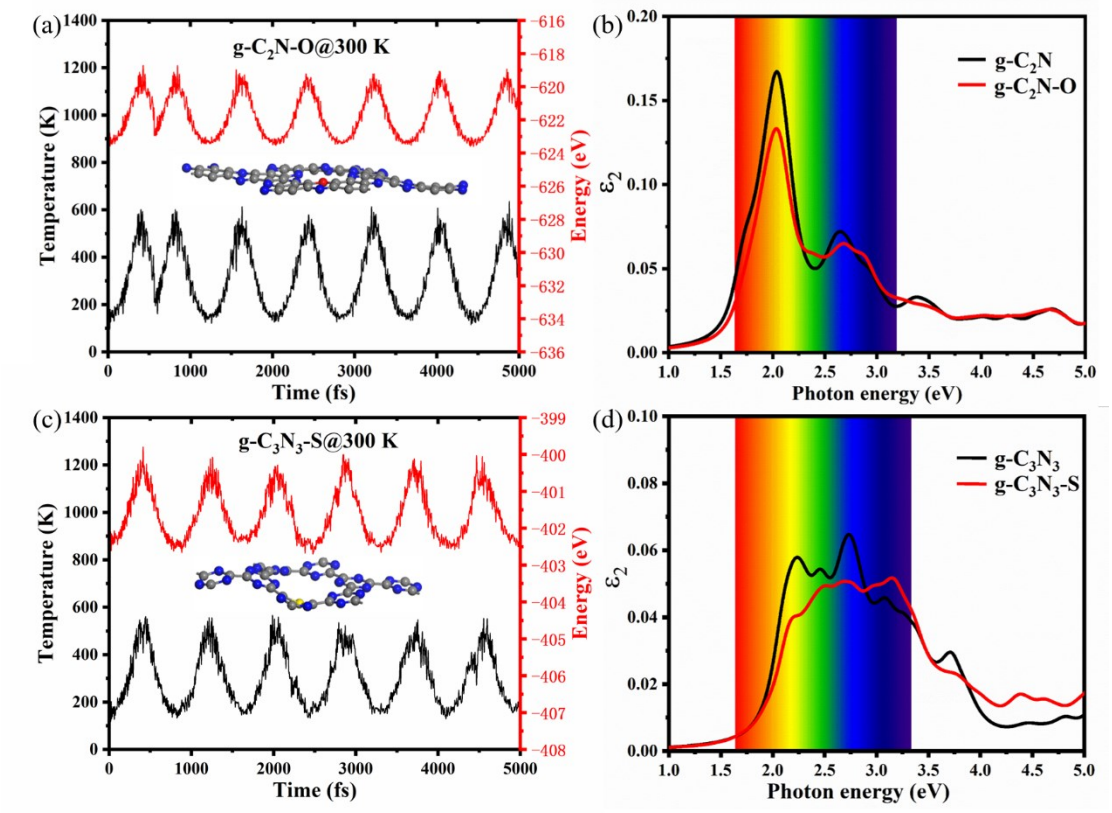

Fig. S40. Energy and temperature fluctuations and one of structures of (a) O-doped g-C_2N and (c) S-doped g-C_3N_3 during 5000 fs; Optical spectrum of (b) pristine g-C_2N and O-doped g-C_2N and (d) pristine g-C_3N_3 and S-doped g-C_3N_3.

1. A. A. Peterson, F. Abild-Pedersen, F. Studt, J. Rossmeisl and J. K. Nørskov, *Energy & Environmental Science*, 2010, **3**, 1311.
2. C. Ling, L. Shi, Y. Ouyang, X. C. Zeng and J. Wang, *Nano Letters*, 2017, **17**, 5133-5139.
3. X. Bai, Q. Li, L. Shi, X. Niu, C. Ling and J. Wang, *Small*, 2020, **16**, 1901981.